1 Introduction

Everything that is not done with utter devotion falls into oblivion and, in fact, does not deserve to be remembered.

Physics and Beyond, Werner Heisenberg

In his delightful small book *An Introduction to Mathematics*, published in 1911, the English mathematician and philosopher Alfred North Whitehead reflected on the role of periodicity in Nature and remarked [1], "The whole life of Nature is dominated by the existence of periodic events, that is, by the existence of successive events so analogous to each other that, without any straining of language, they may be termed recurrences of the same event." He further elaborates, "The presupposition of periodicity is indeed fundamental to our very conception of life. We cannot imagine a course of nature in which, as events progressed, we should be unable to say: 'This has happened before'." It is indeed the case that many natural phenomena manifest *periodic order*. It is enough to consider the rotation of the Earth, the yearly recurrence of seasons, the phases of the Moon, and even the cycles of our bodily life, such as the beatings of our heart or the recurrence of our breathing, as Whitehead observed in his book.

Most likely providing an evolutionary advantage, humans developed the remarkable ability to easily recognize periodic patterns even in the presence of substantial noise and perturbations. In contrast, we perform very poorly at perceiving randomness or at recognizing different degrees of nonperiodic behavior. For instance, when people are asked to assess by inspection the randomness of different binary sequences, it is found that their perceptions simply reflect the inability to efficiently encode them [2]. Experimental psychology has shown that the binary sequences recognized as random invariably contain more alternations between zeros and ones than what are expected for random processes where long runs of zeros or ones that counter the common intuition are occasionally exhibited. Moreover, studies performed by asking people to select integers at random in a given interval demonstrate a systematic bias in favor of smaller numbers, a fact known in cognitive psychology as the "mental compression of large numbers" [3]. Given how deeply rooted in our cognitive structures the idea of periodic order appears to be, it comes as no surprise that such periodic behavior is considered emblematic of structural order.

However, the idea of order without periodicity, or *aperiodic order*, recently began to be fully appreciated thanks to important discoveries in the mathematical and physical sciences. In particular, during the 1920s Harald Bohr developed a general

https://doi.org/10.1017/9781139775328.002 Published online by Cambridge University Press

theory of almost periodic functions that describes the generic quasiperiodic behavior manifested, for instance, by the Lissajous figures for certain choices of parameters. These curves can exhibit intricate patterns arising from the composition of two orthogonal harmonic vibrations, represented as follows:

$$x = A\sin(\omega_1 t + \phi_1) \tag{1.1}$$

$$y = B\sin(\omega_2 t + \phi_2). \tag{1.2}$$

When time progresses, the point P with coordinates (x, y) traces a curve whose shape depends on the choice of the six parameters introduced above. For example, when $\omega_1 = \omega_2$ and the phase difference $\phi_2 - \phi_1 = \pi/2$, the point P traces an ellipse with axes along the x- and y-directions. For an arbitrary phase difference, the ellipse will be tilted and its shape and orientation will vary as a function of the phase difference, switching from a circle (in the case $A = B$) to the straight lines with equations $y = \pm x$, and vice versa. A more complex behavior is obtained when the angular frequencies are different ($\omega_1 \neq \omega_2$). However, as long as their ratio ω_1/ω_2 can be expressed using rational numbers, the corresponding curves eventually repeat themselves, giving rise to an elaborate but periodic motion. Examples are shown in Figure 1.1a–c where we consider frequency ratios of 1, 5/3, and 13/8, respectively. In this example, we also set equal amplitudes ($A = B$) and $\pi/2$ phase difference between the two components.

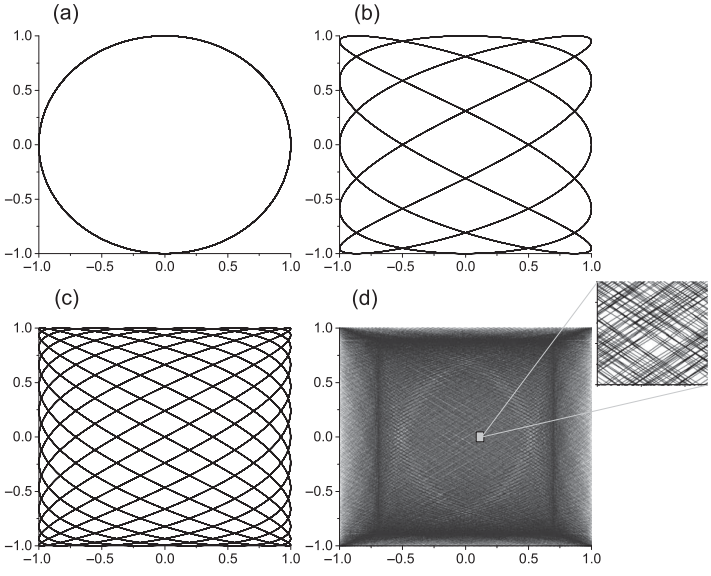

Figure 1.1 Lissajous figures with $A = B$, $\phi_2 - \phi_1 = \pi/2$, and a frequency ratio equal to (a) 1, (b) 5/3, (c) 13/8, and (d) the golden mean τ. The inset in (d) shows a close-up region around the origin of the unit square, highlighting the complex threading of the aperiodic trajectory of point P.

https://doi.org/10.1017/9781139775328.002 Published online by Cambridge University Press

However, the situation changes dramatically when ω_1/ω_2 is irrational, i.e., for incommensurate frequencies. In this case, as shown in Figure 1.1d for ω_1/ω_2 approximately equal to the golden mean $\tau = (1 + \sqrt{5})/2 = 1.618034\ldots$, the trajectory of point P never retraces itself and densely fills the unit square while coming arbitrarily close to every point in a nonperiodic fashion. Since there are many more irrational numbers than rational ones, a random choice for the ratio ω_1/ω_2 will most likely produce nonperiodic trajectories, though with a perfectly deterministic behavior. The simple situation that we have described is typical of the more general quasiperiodic dynamics manifested by conservative systems characterized by a finite number of incommensurate frequencies in their spectra. For instance, as originally recognized by Poincaré at the end of the nineteenth century, the general orbits of the three-body problem of celestial mechanics in which three bodies attract each other gravitationally as in the Earth–Moon–Sun system, are indeed quasiperiodic [4]. Moreover, a fundamental result of dynamics known as the Kolmogorov–Arnold–Moser (KAM) theorem states that such quasiperiodic motions are also stable under small perturbations and therefore represent the norm rather than the exceptional cases. Clearly, this is a remarkable shift from the "presupposition of periodicity." In addition, important milestones in the study of aperiodic order originated from the geometrical theory of tilings or tessellations, which are sets of planar figures that perfectly fill the plane without leaving any gaps. In particular, the mathematician Roger Penrose[1] discovered in 1974 the existence of two simple polygonal shapes that tile, following deterministic prescriptions, the infinite Euclidean plane without any spatial periodicity. Shortly thereafter, generalizations to the three-dimensional (3D) space were provided by Robert Ammann, who produced a pair of rhombohedra that perfectly fill the 3D space without periodicity.

The mathematical models of aperiodic tilings and the theory of quasiperiodic functions found physical applications in the early 1980s in the study of quasicrystals, which are the prototypical examples of perfectly ordered structures without periodicity. Dan Shechtman was awarded the 2011 Nobel Prize in Chemistry for his pioneering work on the electron diffraction of aluminum–manganese alloys that provided the first experimental demonstration of synthetic materials with quasicrystal structures. In 2009, the first known naturally occurring quasicrystal mineral, called icosahedrite, was discovered after a 10-year-long search by an international team of scientists led by Luca Bindi and Paul J. Steinhardt [5].

Today, the phenomenon of aperiodic order plays an important role in several fields of mathematics, biology, chemistry, physics, economics, finance, and engineering where deterministic chaotic systems with long-term unpredictable, though not random, behavior are widespread. For instance, the connection between aperiodic order and unpredictability, which is central to number theory, resulted in numerous engineering applications to cryptography and coding theory. In this context, cryptographically secure deterministic pseudorandom generators (DPRG) have been

[1] Roger Penrose gave numerous pioneering contributions to mathematical physics, particularly in the areas of general relativity and cosmology, and was awarded the Nobel Prize in Physics in 2020 "for the discovery that black hole formation is a robust prediction of the general theory of relativity."

https://doi.org/10.1017/9781139775328.002 Published online by Cambridge University Press

developed that produce numerical sequences featuring statistical randomness (no recognizable patterns or regularities) and exhibit spectral properties that are virtually indistinguishable from those of uncorrelated random noise. Moreover, generating deterministic structures such as automatic sequences by aperiodic substitutions or exploiting number-theoretic concepts such as Galois fields, algebraic rings, or elliptic curves offers novel opportunities for research areas ranging from acoustics diffusers to radar imaging (stealthy surfaces), remote sensing, and photonics technology.

It should be clear from this introductory discussion that a sharp dichotomy between periodic order and random behavior is untenable in view of the recent developments in the field of deterministic aperiodic order leading to the demonstration of novel structures that interpolate in a tunable fashion between periodic crystals and disordered media. Moreover, such a divide has limited our ability to explore and engineer the novel behavior of waves in complex aperiodic media with varying degrees of structural organization, locally defined symmetries, and distinctively rich spatial correlation properties that result in novel wave transport and localization phenomena. Examples discussed in this book include amorphous photonic and hyperuniform media [6], quasicrystals, fractal systems, structures based on automatic sequences [7], and number-theoretic concepts that display inherent chaotic and "random-like" Poisson behavior [8–10].

1.1 Aperiodically Modulated Oscillator Chains

It is remarkable that many important features of the complex behavior of waves in aperiodic systems can already be understood quite generally by considering the vibration modes of one-dimensional systems of harmonic oscillators. Although such "toy models" do not describe actual systems, they quantitatively illustrate the fundamental physical differences in the wave dynamics between periodic and aperiodic structures for both classical and quantum particles.

The simplest dynamical model is the *modulated spring model* consisting of a linear chain of identical particles with nearest-neighbor harmonic interactions described by spring constants that vary along the chain. The spring constants effectively represent atomic interactions in a general material. The relevant equations of motions are given by

$$\frac{d^2u_n}{dt^2} = -\kappa_{n+1}(u_n - u_{n+1}) - \kappa_n(u_n - u_{n-1}), \tag{1.3}$$

where u_n represents the small displacement of a unit mass at position n from its equilibrium. We first discuss the case where spring constants vary according to the following modulation function:

$$\kappa_n = 1 - \epsilon \cos\left(\frac{2\pi a}{b}n + \phi\right) = 1 - \epsilon \cos\left(\frac{2\pi}{N}n + \phi\right). \tag{1.4}$$

https://doi.org/10.1017/9781139775328.002 Published online by Cambridge University Press

The period of the modulation function is $N = b/a$, where a and b are integers, ϕ is the phase shift of the modulation with respect to the chain, and ϵ is the modulation amplitude. The spectrum of the normal modes of vibration is simply obtained by considering the frequency-domain solutions $u_n \sim \tilde{u}_n \exp(-j\omega t)$, where $\tilde{u}_n$ is the spatial envelope of the mode and j denotes the imaginary unit. Substituting into (1.3), we obtain the following eigenvalue problem:

$$\omega^2 \begin{bmatrix} \tilde{u}_1 \\ \tilde{u}_2 \\ \tilde{u}_3 \\ \vdots \\ \tilde{u}_n \end{bmatrix} = \begin{bmatrix} \kappa_1+\kappa_2 & -\kappa_2 & & & \\ -\kappa_2 & \kappa_2+\kappa_3 & -\kappa_3 & & \\ & -\kappa_3 & \ddots & \ddots & \\ & & \ddots & \ddots & -\kappa_{n-1} \\ & & & -\kappa_{n-1} & \kappa_{n-1}+\kappa_n \end{bmatrix} \begin{bmatrix} \tilde{u}_1 \\ \tilde{u}_2 \\ \tilde{u}_3 \\ \vdots \\ \tilde{u}_n \end{bmatrix} \quad (1.5)$$

This problem is defined by a tridiagonal matrix and therefore can be efficiently solved numerically to obtain the spectrum of frequency eigenvalues and the eigenvectors corresponding to the spatial envelopes of the modes at each frequency.

A complete equivalence exists between the modulated spring model and the one in which the masses of the particles are modulated instead, providing a link with the traditional approach to lattice waves in periodic lattices [11, 12]. In particular, when the unit cell of the chain contains N different spring constants or masses ($b = Na$), the modulation function takes on N distinct values, i.e., $\kappa_{n+N} = \kappa_n$ and the solutions of the system (1.5) consist in N frequency branches and $N - 1$ spectral gaps that are opened by the periodic modulation. For example, when $b = 2a$ there will be one gap in the spectrum analogously to the case of a diatomic chain with two distinct masses in the unit cell. Furthermore, when $b = a$ we recover the spectrum of the monoatomic chain, in which there are no gaps. In addition, for a periodic modulation with $b = Na$ the spectral gaps will have maximal width $\Delta\omega \sim \epsilon$ for $\phi = 0$ and will be minimal for $\phi = \pi/N$. In the special case $b = 2a$, the gap will vanish for $\phi = \pi/2$. Therefore, the number of spectral gaps is determined by the factor $2\pi/N$ that appears in the argument of the modulation function. When $N = b/a$ is not an integer, the number of gaps can be found by expressing it as a rational fraction with the smallest denominator. This gives rise to a very large number of gaps when $b \approx a$. Indeed, the number of gaps fluctuates wildly with the values of N for which the oscillation spectrum is computed. Importantly, when $N = b/a$ cannot be expressed as the ratio of two integers, there will be no lattice periodicity in the chain because the spring constants have a period that is incommensurate with the one of the chain. In this case, the equations (1.3) form an infinite set of coupled equations. Since any irrational number can be approximated by rational numbers arbitrarily well, the gap structure can be understood by considering the limit behavior of the spectra for successive rational approximations of N in continued fractions.

A striking consequence of the approximation theory of numbers in rational fractions is that the spectral gaps of the harmonic chain arrange in complex hierarchical structures when we sweep the values $1/N$. As an example of this general phenomenon,

https://doi.org/10.1017/9781139775328.002 Published online by Cambridge University Press

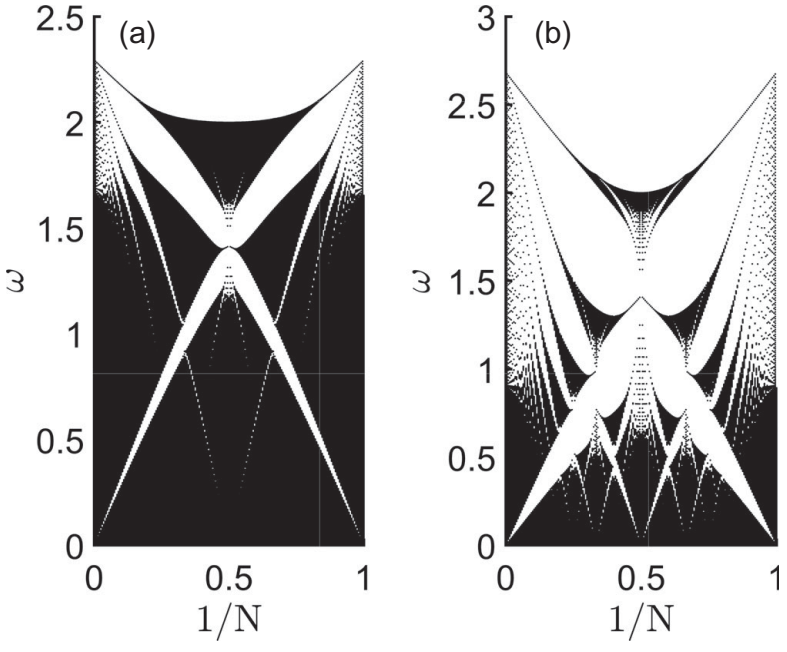

Figure 1.2 Spectrum of the modulated spring model as a function of the modulation period (a) at small modulation amplitude $\epsilon = 0.3$ and (b) at larger modulation amplitude $\epsilon = 0.8$. We considered $\phi = 0$ and 1,000 unit masses.

we show in Figure 1.2 the calculated frequency spectra of the modulated spring model as a function of the inverse period for two different values of the modulation amplitude. The white areas denote the spectral gap regions, while the black ones correspond to transmission states. We recognize that the distribution of largest gap regions is very smooth as a function of $1/N$. In addition, narrower gap regions form visible "branches" that diagonally cross and merge in very complex patterns. Note in particular how the two main "diagonal branches" cross at $1/N = 0.5$, indicating the presence of only one spectral gap, corresponding to the diatomic chain. Additional small gaps can be observed branching off the main diagonal regions with a characteristic self-similar organization that becomes more evident by increasing the modulation parameter ϵ, as shown in Figure 1.2b. Here the same "butterfly-like pattern" appears at multiple scales all over the diagram. Interestingly, this striking recursive structure is also exhibited by the Hofstadter model for the dynamics of a Bloch electron in a crystal under an external magnetic field [13], which in fact has the same mathematical structure of the modulated spring model introduced here [12]. In both cases, when N tends to infinity the total length of the bands goes to zero, producing a "pure-point" spectrum of discrete points.

The transport and spatial localization properties of the different modes depend dramatically on their locations in the spectrum. For instance, transmission eigenstates bounded by large spectral gaps correspond to the extended modes of the system.

https://doi.org/10.1017/9781139775328.002 Published online by Cambridge University Press

In contrast, the very narrow transmission bands embedded in the fragmented spectral regions that are visible in the upper part of the frequency range contain peculiar eigenstates with wildly fluctuating envelopes and an increased localization character. These modes exemplify the characteristic behavior of the *critical modes* that appear in structures with quasiperiodic spring–mass modulations, i.e., obtained when a and b are incommensurate. This scenario corresponds to the Aubry–André or Harper tight-binding model that describes the lattice dynamics of one-dimensional systems in the presence of a gauge field and supports a universal critical behavior characterized by a fractal spectrum with critically localized modes [13–15].

In general, the frequency spectra of incommensurate and quasiperiodic structures are completely determined by the continued fraction expansions of their irrational periods, which produce a self-similar arrangement of spectral gaps forming a Cantor set fractal. A striking example of this intriguing behavior is provided by one-dimensional structures with quasiperiodic modulations that follow the binary Fibonacci sequence. In the context of the modulated spring model, we consider the *Fibonacci chain* defined by the modulation function:

$$\boxed{\kappa_n = \mathrm{sgn}\left[\cos\left(\frac{2\pi n}{\tau} + \phi\right) - \cos\left(\frac{\pi}{\tau}\right)\right].} \tag{1.6}$$

In the preceding expression, τ is the golden mean and sgn denotes the sign operator that makes the modulation binary with $\kappa_n = \pm 1$ values of the spring constant distributed according to the binary Fibonacci sequence. We also remark that by varying the phase angle ϕ we obtain equivalent representations of the Fibonacci chain. Interestingly, the resulting structures flip abruptly when continuously varying ϕ due to the effect of the sgn operation, creating *phason flips*. Moreover, this simple model manifests a complex scenario with interesting topological properties that have been recently discussed in a number of papers [16–18].

In Figure 1.3, we show the integrated density of states (IDOS) of the Fibonacci chain, which is defined as follows:

$$\Omega(\omega) = \int_0^{\omega} \rho(\omega')d\omega', \tag{1.7}$$

where we introduced the *vibrational density of states* that is obtained from the distribution of eigenfrequencies ω_n, as follows:

$$\rho(\omega) = \sum_n \delta(\omega - \omega_n). \tag{1.8}$$

The plateau regions in the normalized IDOS correspond to the spectral gaps of the Fibonacci chain that are distributed in frequency according to a universal fractal staircase function derived from a Cantor set. Remarkably, the self-similarity of the Fibonacci spectrum is largely independent of the specific physical nature of the

https://doi.org/10.1017/9781139775328.002 Published online by Cambridge University Press

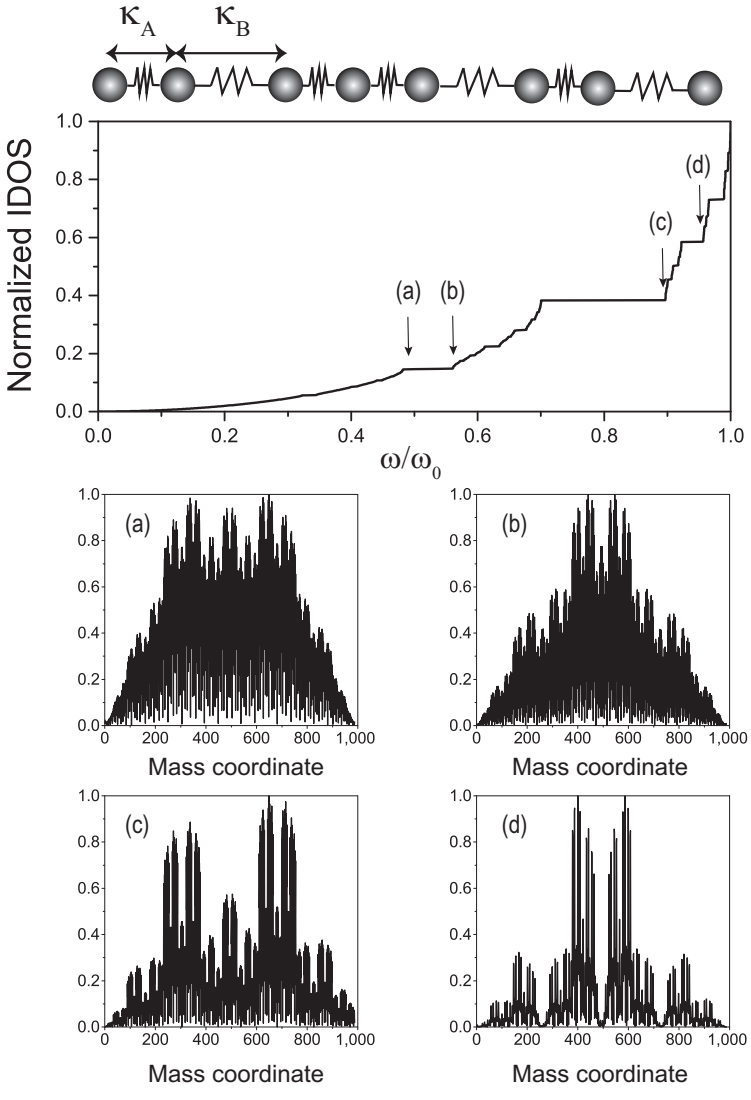

Figure 1.3 Top: integrated density of states of a Fibonacci harmonic chain of 978 masses. Panels (a–d) show the spatial profiles of the selected vibration modes at the frequency positions indicated by the corresponding arrows in the top panel.

system and only reflects the self-similar process of continued fraction expansion of the incommensurate modulation period of the chain:

$$\tau = 1 + \cfrac{1}{1 + \cfrac{1}{1 + \cfrac{1}{1 + \ddots}}} \tag{1.9}$$

https://doi.org/10.1017/9781139775328.002 Published online by Cambridge University Press

In particular, each level of fractional approximation of the golden mean, i.e., each approximant value, is responsible for the splitting of one frequency band into two sub-bands with a width proportional to the corresponding approximant. However, the actual width of each fractal sub-gap will also depend on the actual modulation amplitude. We note that in the low-frequency regime, the normalized IDOS is almost identical to the one of a periodic chain and the corresponding modes are extended. On the other hand, in the high-frequency regime, the IDOS becomes self-similar with a dense set of gaps and critical modes that exhibit increasing spatial localization. In Figure 1.3, we plot four representative (normalized) vibration modes obtained by the direct diagonalization of the harmonic spring model with Fibonacci modulation. These eigenvectors are critical band-edge modes characterized by distinctive envelope fluctuations with multifractal scaling properties, as demonstrated using wavelet analysis in the next section. The fractal dimensions of the critical modes and of the frequency spectra of 1D quasiperiodic structures determine the asymptotic scaling of the width of a spreading wave packet, resulting in anomalous diffusion properties [19–22].

The peculiar hierarchical structure of critical modes can be quite generally understood on the basis of the *Conway theorem* [23]. This result states that every finite region of characteristic length L in a quasicrystal admits at least one identical replica within a distance $\sim L$. As a result, the frequent and regular reappearances of identical local environments along the Fibonacci chain give rise to tunneling of exponentially localized wave packets from one cluster to its nearby copies in the structure, forming the characteristic critical mode envelopes displayed in Figure 1.3. The distinctive spatial decay of the critical modes in quasicrystal of size L is characterized by considering the scaling with respect to L of the number $N(\epsilon)$ of sites in the structure where $|u_n|^2$ exceeds a small threshold ϵ [11]. We note that for periodic structures $N(\epsilon) \sim L$ because they support extended modes with roughly equal intensity at all sites. On the other hand, $N(\epsilon)$ is bounded by a constant in random structures supporting localized states, since their intensity will vanish almost everywhere except for a few sites. In contrast, for critical states we have that $N(\epsilon) \sim L^{\alpha}$ with $0 < \alpha < 1$. According to this criterion, we say that critical modes display a power-law spatial decay that is intermediate between extended and exponentially localized states.

1.2 A Brief History of Aperiodic Optics

The optical properties of periodic and disordered random media have been deeply investigated for centuries, leading to a number of spectacular physical effects that unveil deep analogies between the behavior of quantum and electromagnetic waves [24–27]. The first scientific analysis of waves on a periodic lattice of one-dimensional oscillators, i.e., the spring–mass model, can be traced back to Newton in his attempt to derive a mathematical expression for the velocity of sound. A general theory of wave propagation in periodic structures can already be found in the work of Brillouin [28]. On the other hand, the radiative transfer equation (RTE) for the propagation of light in randomly structured (turbid) media consisting of isotropically scattering centers was

https://doi.org/10.1017/9781139775328.002 Published online by Cambridge University Press

first introduced in 1887 by Eugen von Lommel [29], and subsequently generalized to include arbitrarily polarized waves by Chandrasekhar [30]. However, the radiometry of randomly structured media has a long and fascinating history that dates back to the pioneering works of Pierre Bouguer and Johann Lambert around the middle of the eighteenth century [29]. In contrast, the propagation of optical waves in strongly scattering aperiodic media is a rather recent field of study. In fact, it was not until the pioneering work of Anderson on quantum and classical wave scattering in disordered media that profound questions on the nature of wave transport in aperiodic media began to be directly addressed [31, 32]. One of the first phenomena to be investigated in this context was the coherent backscattering of light [33–35], or *weak localization*, which is a direct manifestation of wave interference in photon transport. During the 1980s, intense research activities focused on the search for Anderson light localization [32, 36], where wave propagation in a random medium is dominated by interference effects and light transport can be completely suppressed.

In 1984, Dan Shechtman et al. [37] demonstrated experimentally the existence of physical structures with noncrystallographic rotational symmetries. In their study of the electron diffraction spectra from certain metallic alloys (Al_6Mn), they discovered sharp diffraction peaks arranged according to the icosahedral point group symmetry. The sharpness of the measured diffraction peaks, which is a measure of the coherence of the spatial interference, turned out to be entirely comparable with what typically observed in ordinary periodic crystals. Intrigued by these findings, Dov Levine and Paul Steinhardt promptly formulated the notion of quasicrystal in a seminal paper titled [38]: "Quasicrystals: a new class of ordered structures." It then became apparent that icosahedral structures can be obtained by projecting periodic crystals from a higher-dimensional (six-dimensional in this case) superspace, which became a central idea in geometrical diffraction theory and quasicrystallography [11, 39, 40].

1.2.1 One-Dimensional Aperiodic Structures

The first study of electron transport across a one-dimensional (1D) quasiperiodic Fibonacci structure was performed by Merlin et al. [41] in 1985. This work stimulated a flurry of experimental and theoretical work on the propagation of electron waves through quasiperiodic media. Largely stimulated by these results, the interest in quasiperiodic photonic structures began in 1987 with the first investigation of 1D dielectric multilayers arranged in a Fibonacci sequence [42]. Such structures display a very complex transmission spectrum characterized by a hierarchical organization of pseudogap regions and support resonant states with fractal scaling properties that are similar to what were previously discussed for the modulated spring model. In fact, photonic quasicrystals of the Fibonacci type exhibit an energy spectrum that consists of a self-similar Cantor set with zero Lebesgue measure, implying the presence of narrow transmission pseudogaps with vanishingly small widths in the limit of infinite-size systems.

The transmission spectrum of transverse electric (TE) waves through a photonic multilayer medium constructed by arranging two types of layers according to a

https://doi.org/10.1017/9781139775328.002 Published online by Cambridge University Press

prescribed deterministic sequence can be conveniently calculated using the standard transfer matrix technique [43]. In this method, the amplitudes of the electric and magnetic field vectors on the two sides of a dielectric layer with thickness d_i and refractive index n_i are related through the transfer matrix:

$$\begin{bmatrix} E_\ell \\ B_\ell \end{bmatrix} = \mathbf{M}(d_i) \begin{bmatrix} E_r \\ B_r \end{bmatrix} = \begin{bmatrix} \cos\delta_i & -jp_i^{-1}\sin\delta_i \\ -jp_i\sin\delta_i & \cos\delta_i \end{bmatrix} \begin{bmatrix} E_r \\ B_r \end{bmatrix}, \tag{1.10}$$

where the indices ℓ and r refer to the left and right interfaces of the layer, $\delta_i = k_0 n_i d_i \cos\theta_i$ is the phase change of layer i when the light makes an angle θ_i with the normal to the interface, and $p_i = n_i/c_0 \cos\theta_i$ (k_0 is the wave vector and c_0 the speed of light in vacuum). By imposing the continuity conditions of the electric and magnetic fields, we can construct the transfer matrix $\mathbf{M}_N$ for a system with N layers by the matrix multiplication:

$$\mathbf{M}_N = \prod_{i=1}^{N} \mathbf{M}(d_i) = \begin{bmatrix} M_{11} & M_{12} \\ M_{21} & M_{22} \end{bmatrix}. \tag{1.11}$$

If p_0 and p_m are the values of p_j for the incident and transmitted waves, respectively, then the transmissivity T can be expressed as [43]:

$$T = \frac{4p_0 p_m}{p_0^2 M_{11}^2 + p_m^2 M_{22}^2 + (p_0 p_m)^2 |M_{12}|^2 + |M_{21}|^2 + 2p_0 p_m}. \tag{1.12}$$

For a 1D multilayer system, it is also possible to compute the electric field distribution inside the structure. In order to achieve this, we first need to calculate the reflectivity coefficient of the whole structure, after which the incident and the total reflected light can be used as boundary conditions to obtain the field amplitude of all layers inside the structure. The electric field on the kth interface can be expressed as follows [44]:

$$E(z^{(k)}, \omega) = [1 + r(\omega)] m_{22}^{(k)} - p_0 [1 - r(\omega)] m_{12}^{(k)}, \tag{1.13}$$

where $m_{ij}^{(k)}$ are the elements of the transfer matrix from the first to the k-th interface.

It can be shown that the recursive structure of the Fibonacci numbers given by $F_{j+1} = F_j + F_{j-1}$ for $j \geq 1$ with $F_0 = F_1 = 1$ gives rise to a corresponding recursion of the transfer matrices:

$$\mathbf{M}_j = \mathbf{M}_{j-2} \mathbf{M}_{j-1}, \tag{1.14}$$

where $\mathbf{M}_j$ is the transfer matrix of a Fibonacci structure with F_j layers [42]. Equation (1.14) has been shown to be equivalent to the *dynamical map*:

$$x_{j+1} = 2x_j x_{j-1} - x_{j-2}, \tag{1.15}$$

where $x_j = (\mathrm{Tr}\,\mathbf{M}_j)/2$ denotes half the trace of the transfer matrix and the allowed frequencies in the spectrum generally satisfy the constraint $-1 \leq x_j \leq 1$ [45, 46]. The dynamical map has a constant of motion that quantifies the strength of the

https://doi.org/10.1017/9781139775328.002 Published online by Cambridge University Press

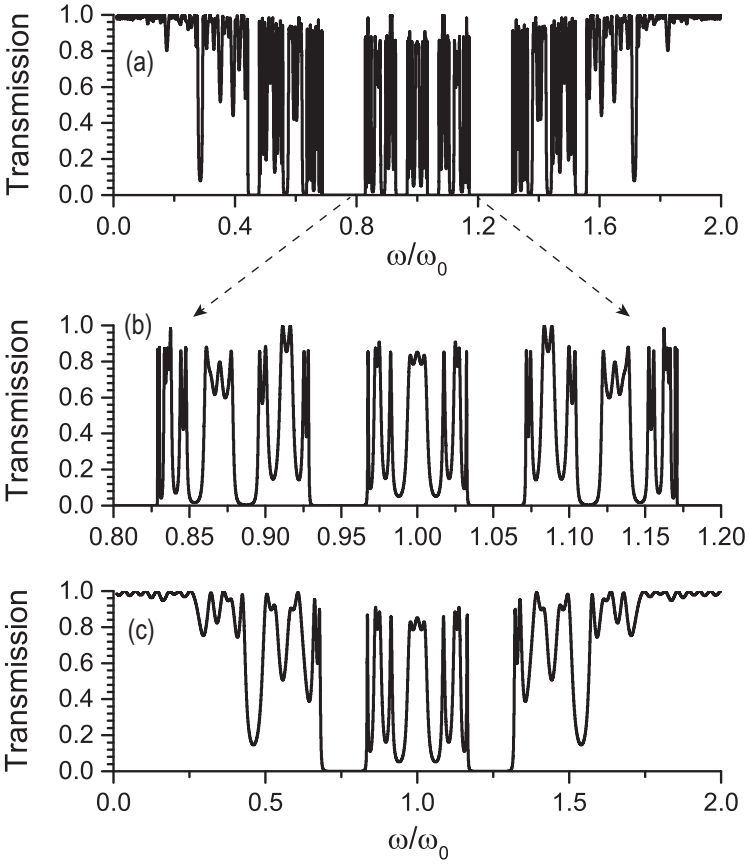

Figure 1.4 Scaling of Fibonacci spectra. (a) Optical transmission spectrum of a Fibonacci multilayer structure with 233 layers as a function of the normalized frequency where $\omega_0 = 2\pi c_0/\lambda_0$; and (b) enlarged view of the spectrum to around the scaling region $\omega/\omega_0 \approx 1$. (c) Optical transmission spectrum of a Fibonacci multilayer structure with 55 layers. The A and B symbols denote two dielectric layers with refractive indices $n_A = 2$ and $n_B = 3$ and optical thickness determined by the $\lambda/4$ Bragg condition.

effect of quasiperiodicity and is maximized at the quarter-wavelength layer condition ($n_i d_i = \lambda_0/4$) [42, 45]. Moreover, under such condition the cyclic character of the Fibonacci trace map implies that the transmissivity $T(S_j)$ of the Fibonacci structure S_j repeats every three generations of the sequence, i.e., $T(S_{j+3}) = T(S_j)$, and exhibits a self-similar behavior around $\delta = \pi/2$, as shown in Figure 1.4 [42, 47]. The self-similarity of the transmission spectrum of Fibonacci dielectric multilayers was first demonstrated by Gellerman et al. [47]. The fractal nature of the energy and of the transmission spectra of Fibonacci photonic quasicrystals drastically modifies the dynamics of optical wave packets, resulting in largely tunable anomalous transport properties [19, 20, 22]. Moreover, the critical modes of photonic quasicrystals exhibit multiscale intensity fluctuations described by multifractal geometry, similarly to the

https://doi.org/10.1017/9781139775328.002 Published online by Cambridge University Press

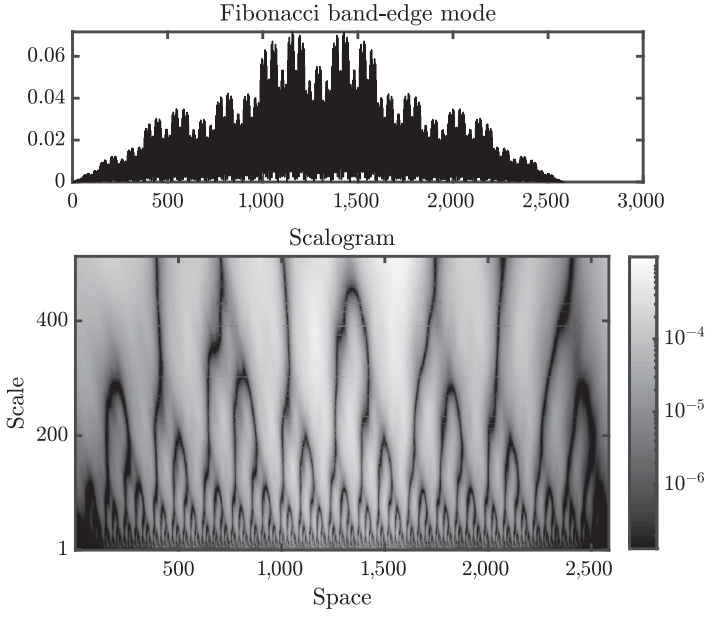

Figure 1.5 Wavelet-based scalogram of the first band-edge mode (shown in the top panel) of an optical Fibonacci multilayer (1,597 layers). The self-similar nature of the critical mode oscillations is displayed clearly by the scalogram (shown in the bottom panel).

wave functions of random media at the Anderson localization transition [48–50]. This is visibly demonstrated by the self-similar structure of the wavelet scalogram of the first band-edge optical mode in a Fibonacci quasicrystal, as shown in Figure 1.5. Wavelet-based techniques for self-similarity detection and multifractal analysis are introduced in Chapter 9. Here we remark the impressive similarity between the optical mode shown in the top panel of Figure 1.5, which is the mode of an optical system, and the one shown in Figure 1.3, which is a vibrational band-edge mode of the harmonic Fibonacci chain. Despite the very different physical nature of the two systems, their critical mode patterns are virtually identical, demonstrating the primary role played by the Fibonacci quasiperiodic modulation. This fact generalizes to other 1D aperiodic structures as well, such as, for instance, the ones with the binary Thue–Morse modulation defined recursively by the following:

$$\epsilon_0 = 0, \;\; \epsilon_{2n} = \epsilon_n, \;\; \epsilon_{2n+1} = 1 - \epsilon_n. \tag{1.16}$$

The preceding equations generate an infinite binary string of digits that never repeat. The same string can alternatively be generated by the simple substitution rule: $0 \rightarrow 01$, $1 \rightarrow 10$, and several other characterizations exist as well [51]. Interestingly, the Thue–Morse sequence remains invariant upon the decimation of every other digits, and therefore it is not only aperiodic but also self-similar.

After the breakthrough discovery of quasicrystals and the fabrication of Fibonacci as well as Thue–Morse semiconductor heterostructures [41, 52], it became clear that

https://doi.org/10.1017/9781139775328.002 Published online by Cambridge University Press

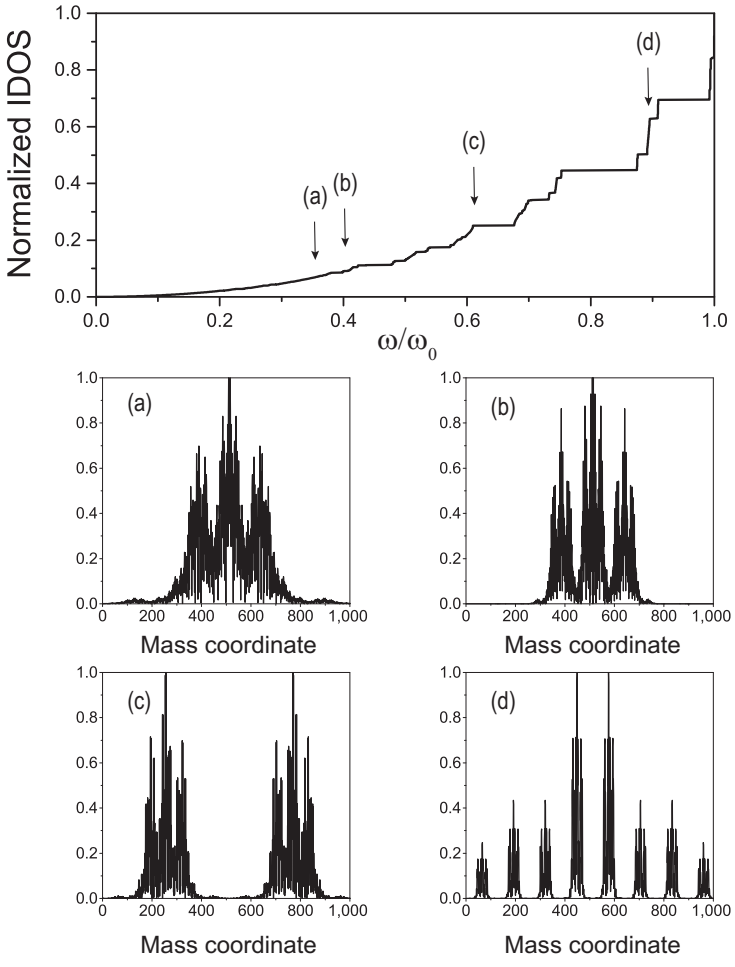

Figure 1.6 Top: integrated density of states of a Thue–Morse harmonic chain of 1,024 masses. Panels (a–d) show the spatial profiles of the selected vibration modes at the frequency positions indicated by the corresponding arrows in the top panel.

physical systems could be engineered with singular-continuous energy spectra not previously encountered in any natural system. Figure 1.6 summarizes the relevant properties of the Thue–Morse harmonic chain. A fractal distribution of gaps similar to the case of the Fibonacci chain appears in the IDOS of the Thue–Morse structure and the critically localized modes shown in Figure 1.6a–d demonstrate a characteristic triplication pattern. Similar results are obtained for optical multilayers as well [53–56].

1.2.2 Energy Spectra and Nonlinear Dynamics

Seminal work on the nature of the electronic and optical spectra of Fibonacci structures and the properties of the corresponding eigenmodes was performed by Kohmoto,

https://doi.org/10.1017/9781139775328.002 Published online by Cambridge University Press

who established an exact isomorphism between the 1D Schrödinger equation with aperiodic electron potentials and the Helmholtz equation for classical waves [42, 45, 57]. In these papers, a transfer matrix method was utilized that enabled the exact treatment of 1D scattering problems for electronic and optical excitations on the same footing. An alternative approach was also introduced by Kohmoto, Kadanoff, and Tang [58, 59] that exploits the recursion relations of the transfer matrices to define an iterative map for their traces and antitraces, leading to the efficient calculation of the energy spectra of large-scale 1D aperiodic structures. The resulting formalism, known as the *trace map* approach, describes the physical properties of deterministic aperiodic structures by analyzing the orbits of corresponding discrete dynamical systems [60]. The study of the trace map of aperiodic structures enables the computation of their spectrum without calculating the full product of matrices, thus significantly reducing the complexity of the problem. Considering the nonlinear nature of these dynamical systems, Kohmoto and Oono [61] were able to discover the Smale horseshoe mechanism, which is considered the hallmark of chaos in dynamical systems theory, in the trace map of Fibonacci multilayers. Wave propagation through Cantor-set fractal media and its relation to chaos theory is discussed in the recent paper by Esaki et. al. [62]. In particular, it was demonstrated that the phase-space trajectories of the trace map and their basins of attraction in the two-dimensional trace space (or a higher-dimensional) space provide universal information on the nature of resonant states and transmission spectra in quasiperiodic structures. This very elegant method has been also extended to more complex aperiodic systems, such as the Thue–Morse structure and its generalizations [51] as well as the generalized Fibonacci structures (GFS). The GFS are defined following the inflation scheme [63]:

$$S_{j+1} = S_j^m S_{j-1}^n, \tag{1.17}$$

where, for instance, $S_0 = B$ and $S_1 = A$, m and n are integers, and S_j^m denotes m adjacent repetitions of the string S_j. This inflation scheme is equivalent to the substitution rule $A \rightarrow A^m B^n$, $B \rightarrow A$, where A^m is a string of m A's. The total number of A's and B's is the string S_j is equal to the *generalized Fibonacci number* F_j defined by the recurrence relation $F_j = mF_{j-1} + nF_{j-2}$ with $F_0 = F_1 = 1$. In these structures, the ratio of A's and B's for $j \rightarrow \infty$ is $\tau' = \sigma/n$, where

$$\sigma = \lim_{j\rightarrow\infty} \frac{F_j}{F_{j-1}} = \frac{1}{2}[m + \sqrt{m^2 + 4n}]. \tag{1.18}$$

When $m = n = 1$, we obtain the standard Fibonacci sequence and τ' reduces to the golden mean τ. However, when $m = 2$ and $n = 1$, we obtain the so-called *silver mean sequence* with $\sigma = 1 + \sqrt{2}$; when $m = 3$ and $n = 1$, we obtain the *bronze mean sequence* with $\sigma = (3 + \sqrt{13})/2$; when $m = 1$ and $n = 2$, we have the *copper mean sequence* with $\sigma = 2$; and finally, when $m = 1$ and $n = 3$, we obtain the *nickel mean sequence* with $\sigma = (1 + \sqrt{13})/2$. Similarly, the Thue–Morse sequence can be generalized following the substitution rule $A \rightarrow A^m B^n$, $B \rightarrow B^n A^m$. In this case, the ratio of A and B letters in the sequence is equal to m/n. Differently from the Fibonacci case, these systems are characterized by two-dimensional, nonlinear,

https://doi.org/10.1017/9781139775328.002 Published online by Cambridge University Press

and area nonpreserving trace maps and exhibit a degree of aperiodicity intermediate between quasiperiodic and random systems.

In order to illustrate the main ideas behind the trace map method we consider the trace map of the standard Thue–Morse sequence [51]:

$$x_{j+1} = y_j \tag{1.19}$$

$$y_{j+1} = 4x_j^2(y_j - 1) + 1 \tag{1.20}$$

and the one of the copper mean sequence [46]:

$$x_{j+1} = y_j \tag{1.21}$$

$$y_{j+1} = (4x_j^2 - 2)y_j + \gamma, \tag{1.22}$$

where γ is a parameter. Depending on the regions of trace space, these maps may exhibit bounded or unbounded orbits, periodic points, and attractors with very complex and even fractal shapes. However, these maps provide access to properties of the corresponding systems that are completely independent of the nature of the transfer matrices associated to the binary blocks A and B in the structures. In fact, the energy spectra of any 1D physical system specified by unimodular transfer matrices, such as an electronic or an optical multilayer structure, can be accurately computed simply considering the dynamical properties of the maps. This is so because the allowed energy bands are always characterized by stable orbits and fixed points. Therefore, to find the spectra of a given model it will suffice to plot the curve generated by the initial values of the traces (x_1, y_1) as a function of energy (or optical phase β) and look for intersections with various regions of the *fractal basins of attraction* of the trace map. Given the chaotic nature of the fractal basins of attraction,[2] the transmission spectra of aperiodic 1D structures generally display very irregular distributions of peaks and gaps with remarkable scaling properties. Following this general method, one can predict exactly the transmission spectra without ever iterating the trace map. In Figure 1.7, we show the transmission spectra of dielectric multilayer structures corresponding to (a) the Thue–Morse sequence, (b) the copper mean sequence, and (c) the silver mean sequence. A complex structure of nested gaps and transmission states populate the frequency space of these remarkable structures.

We now illustrate how the trace map approach can be used the determine the transmission spectra of the Thue–Morse and the copper mean optical multilayer structures assuming for simplicity that $\beta_j = \beta$ for all j. In the case of the Thue–Morse multilayer, the initial conditions for the trace map can be readily obtained from the optical transfer matrices and the trajectory of the point $(x_1(\beta), y_1(\beta))$ in the (x, y) trace space defines a parabolic curve. The special values of the optical phase β that correspond to transmission peaks are then found by finding the intersections of such parabola of initial trace values with the subset of the basin of attraction of the point $(1, 1)$, for the given number of generations of the predecessors of the $(1, 1)$ point [51].

[2] The basin of attraction of the map for a given stable point is the set of points in trace space that are mapped to that point upon iteration.

https://doi.org/10.1017/9781139775328.002 Published online by Cambridge University Press

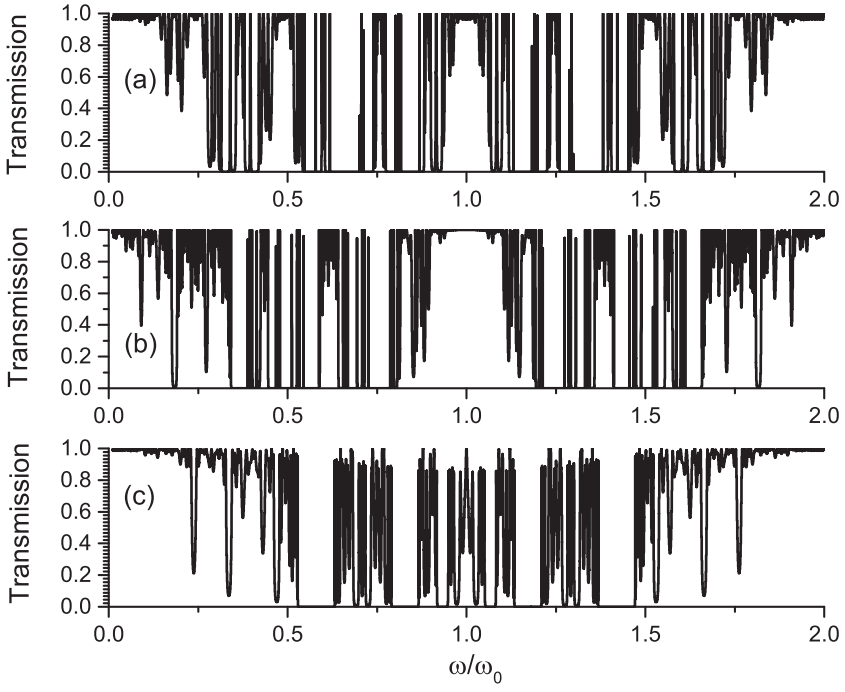

Figure 1.7 Transmission spectra of optical multilayer structures with aperiodic distribution of layers according to the (a) Thue–Morse sequence, (b) the copper mean sequence, and (c) the silver mean sequence. The A and B symbols denote two dielectric layers with refractive indices $n_A = 2$ and $n_B = 3$ and optical thickness determined by the $\lambda/4$ Bragg condition.

The case for 12 generations of the predecessors is shown in Figure 1.8a, where the invariant parabola is indicated in gray color. The outstanding complexity and chaotic behavior of the basin of attraction is evident in the figure. On the other hand, in order to find the transmission peaks of copper mean structures, we need to compute the basin of attraction of the $y_\ell = 0$ line in trace space for the corresponding trace map [46]. We then proceed as in the Thue–Morse case and look for the intersections of the basin of attraction with the invariant curve of initial conditions. In the case of the copper mean map, the invariant curve is a Lissajous figure with the parametric representation $\{\cos t, \cos(2t - \alpha)\}$ with $\cos\alpha = \gamma$ and $t \in (0, 2\pi)$. The chaotic attractor of the copper mean map is shown in Figure 1.8b for the first eight generations of predecessors of $y_\ell = 0$ and the invariant Lissajous curve is highlighted in gray.

The dynamical trace map approach was also applied to investigate the properties of arbitrary substitutional sequences by Kolář and Nori [64]. The rich physical behavior of critical states, including the presence of extended fractal wavefunctions at the band-edge energy of the Fibonacci spectrum, and their relation to optical transport are analytically studied by Kohmoto and Maciá-Barber using rigorous discrete tight binding method and a transfer matrix renormalization technique, respectively [59, 65]. The existence of critical modes in quasiperiodic Fibonacci systems was

https://doi.org/10.1017/9781139775328.002 Published online by Cambridge University Press

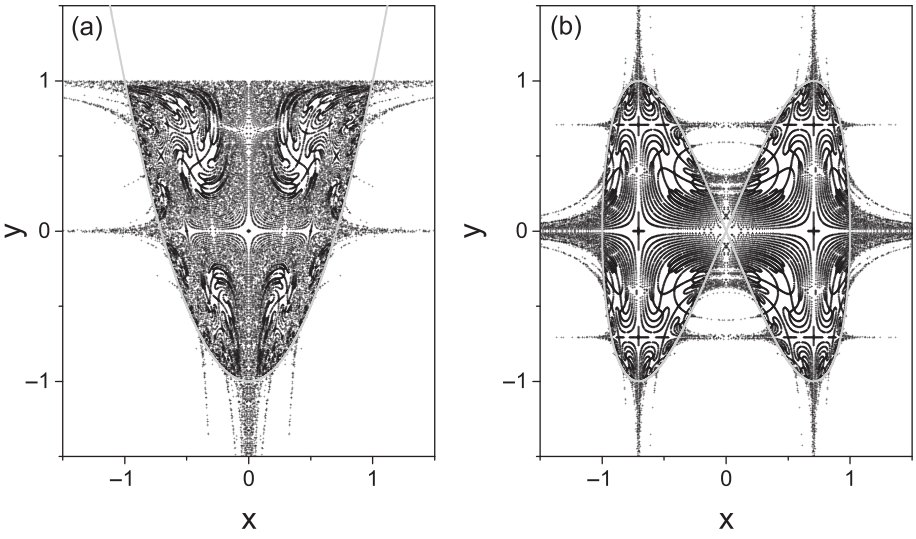

Figure 1.8 (a) Basin of attraction of the Thue–Morse map (black crosses). The first 12 generations of the predecessors of the point $(1, 1)$ and the invariant parabola (gray curve). (b) Basin of attraction of the copper-mean map with $\gamma = 0$ (black crosses). The first eight generations of the predecessors of the $y_\ell = 0$ line and (gray curve) the invariant Lissajous figure.

demonstrated experimentally by Desideri and coworkers [66] who investigated the propagation of Rayleigh surface acoustic waves on a quasiperiodically corrugated solid. Characteristic spatial patterns with remarkable scaling features were shown from optical diffraction experiments [67]. The complex photonic dispersion of optical waves transmitted through a Fibonacci multilayer structure was demonstrated experimentally by Hattori and coworkers [68] while Dal Negro and collaborators used ultrashort pulse interferometry to demonstrate strongly suppressed group velocity at the Fibonacci band-edge states [44]. Recently, the optical properties of multilayered structures based on the Thue–Morse sequence, characterized by a singular continuous Fourier spectrum, have also attracted considerable attention [51, 53, 54, 69]. These structures are characterized by a self-similar hierarchy of optical gaps that scale according to a triplication pattern of symmetry-induced perfect transmission states [53], as shown in Figure 1.6 for the harmonic Thue–Morse chain.

In applied optics and photonics, aperiodic optical media generated by deterministic mathematical rules attract significant interest due to their simplicity of design, fabrication, and full compatibility with current materials deposition and device technologies. In particular, deterministic aperiodic nanostructures (DANS) generated by substitution rules and number-theoretic functions have been recently demonstrated, and technological applications have been found in different areas of nanophotonics and plasmonics in relation to improved optical sensing, spectroscopy, broadband light sources, lasers, and nonlinear optical elements [70–74].

https://doi.org/10.1017/9781139775328.002 Published online by Cambridge University Press

1.3 Scope of This Book

The study of waves in complex media deals with a broad spectrum of electromagnetic scattering phenomena that occur in structurally aperiodic environments composed of resonant optical materials, with applications to both photonic technology and fundamental optical science. Also known as *complex photonics*, this fascinating research field combines electromagnetic scattering and diffraction theory in dispersive materials with the mathematical characterization and design of structures that lack periodicity and instead manifest aperiodic spatial correlations [75]. The present book provides a multidisciplinary and comprehensive introduction to the single and multiple scattering properties of electromagnetic waves in complex media, with emphasis on the foundational aspects of aperiodic order that play an important role in applied and basic optical science. This graduate-level textbook introduces the wave physics and engineering of both disordered and deterministic aperiodic media that interpolate in between periodic crystals and random structures. Besides providing a self-consistent discussion of the analytical framework of single and multiple light scattering theory, this book attempts to integrate a vast number of recent results and developments into a coherent story that balances electromagnetic physics, engineering design concepts, mathematical ideas, and advanced device applications to metamaterial, photonic, and plasmonic technologies.

In order to achieve these goals, the book systematically introduces and develops all the concepts and techniques that are essential to understand the complex behavior of light waves in aperiodic and random media without requiring prior knowledge on the subjects beyond what is normally acquired in the undergraduate physics and engineering curricula. The wide spectrum of selected topics is developed to position graduate students in the conditions to deepen their understanding of physical phenomena in strong partnership with semi-analytical design and modeling techniques for waves in complex media. The combination of conceptual aspects and rigorous design of complex media will allow students to directly engage with the more specialized literature on the subject. Key concepts and results of single scattering and multiple scattering theories of scalar and vector waves, which are essential tools for every researcher, are introduced and developed at the graduate level. The emphasis is on analytical formulations and general results, since they provide physically transparent insights into the complexities of aperiodic optics and serve as rigorous starting points for many numerical techniques utilized to study complex optical media. Moreover, our interdisciplinary detours into several mathematical aspects of the subject in combination with extensive references to device applications should also appeal to practitioners in both industry and academia who may approach complex wave phenomena from different disciplines, including mathematics, physics, astronomy, engineering, and biology.

We begin by providing in Chapter 2 the background concepts of classical electromagnetic field theory. In particular, we start from Maxwell's equations in free space and discuss fundamental theoretical concepts, such as the radiation potentials and the connection between the Green function and the density of states in optical systems. We then introduce macroscopic fields and the macroscopic Maxwell's equations

https://doi.org/10.1017/9781139775328.002 Published online by Cambridge University Press

needed for the classical description of the optical behavior of materials. We then proceed to discuss different field representations and wave equations in materials. The dyadic formalism is introduced in the context of a general radiation and scattering problem whose solution is provided by volume integral equations in terms of the dyadic Green function. The resonant response of dispersive materials is often a key element in the description of strongly scattering media, requiring the formulation of dispersion models introduced in Chapter 3. Here we rigorously analyze the behavior of waves in dispersive media and introduce polariton waves, which play a central role in current nano-optical technology. This leads us to discuss the effective optical response of heterogeneous complex media made of small scattering inclusions and introduce the idea of electromagnetic metamaterials. In Chapter 4, we study the propagation of optical wave packets through dispersive media and introduce the basic equations of pulse dynamics along with a powerful solution approach based on neural networks. We then proceed with a discussion of scalar diffraction theory including the modern formulation based on the angular spectrum representation of waves. This chapter also introduces an alternative formulation of paraxial light diffraction based on the fractional Fourier transform and concludes with a brief account of the Stratton–Chu integral formula in the context of vector diffraction theory. Design concepts and advanced engineering applications of optical diffraction are discussed in Chapter 5 within the elegant framework of linear systems theory. In particular, complex diffractive optical elements are presented with application to both space and time domains. Structural complexity in diffraction theory is addressed in the last two sections, where we introduce the general framework of catastrophe optics and provide several examples of engineered caustics. Finally, optical rogue waves in aperiodic diffractive media are introduced and the fascinating concepts of singular optics and meta-optics are briefly introduced. Chapter 6 introduces the general formalism of wave scattering theory for both perfectly and partially coherent fields. The basic concepts of the unified theory of coherence and polarization are summarized and their applications to the scattering of partially coherent radiation by deterministic and random media are provided.

The fundamental connection between wave diffraction and the kinematic scattering theory is addressed in Chapter 7, where we establish the physical and geometrical meaning of the structure factor for arbitrary arrays of scattering particles and provide numerous examples to radiation engineering using deterministic aperiodic structures. This chapter introduces the main spectral types of deterministic aperiodic structures in one spatial dimension and addresses their diffraction properties. Chapter 7 closes with a discussion of the resonant behavior of periodic arrays of nanoholes and nanoparticles that found with numerous device applications in relation to the extraordinary light transmission properties of periodically nanostructured metallic surfaces. In Chapter 8, we address the important topic of tailored disorder and introduce the statistical description of random media. The effects of long- and short-range spatial correlations are discussed starting from a brief introduction to optical speckles and correlated random walks. This chapter introduces the concepts of hyperuniform random and deterministic media based on engineered subrandomness and discusses their application to the design of weakly scattering and stealthy media.

https://doi.org/10.1017/9781139775328.002 Published online by Cambridge University Press

The following three chapters provide an interdisciplinary journey through number theory and diffraction geometry to explore randomness and aperiodic order at its conceptual roots. In Chapter 9, we introduce arithmetic functions and analyze their distinctively multiscale aperiodic behavior using multifractal scaling analysis. We then focus on the Riemann zeta function and the aperiodic distribution of prime numbers, as well as surprising connections with chaotic systems and the theory of random matrices. Finally, we introduce the relevant notions of continued fractions and Diophantine approximation theory that often appear in the rigorous analysis of aperiodic order. Chapter 10 deals with quasiperiodicity and the Poisson behavior in number theory, and it exploits "arithmetic randomness" for the design of novel aperiodic point patterns. Aperiodic arrays based on prime numbers are then introduced along with the relevant concepts from algebraic number theory. The aperiodic structures of Galois fields and elliptic curves (over finite fields) are presented together with deterministic methods that efficiently generate weak and strong pseudorandomness. Chapter 10 ends with a broader discussion of the concept of randomness in the contexts of algorithmic information theory and statistical analysis. The Fourier spectral properties of aperiodic point patterns are discussed in Chapter 11 in the general context of diffraction geometry, and the main classes of aperiodic structures are discussed together with their mathematical diffraction properties. Quasicrystals and the approach of higher-dimensional quasicrystallography are introduced as well as additional types of aperiodic structures from phyllotaxis and number theory.

In Chapter 12, we return to wave scattering physics and introduce the powerful method of Green's function perturbation theory. Within this general framework, we derive the multiple scattering equations for scalar and vector electromagnetic waves and introduce the coupled dipole numerical technique for the design of scattering arrays of electric and magnetic dipoles. The dyadic Green's matrix method is introduced and applications to the multiple scattering physics of different types of deterministic aperiodic media are provided. In particular, we show how the analysis of the spectral properties of the dyadic Green's matrix provide invaluable information on the wave transport and localization properties of large aperiodic scattering arrays. The resonant scattering properties of particles beyond the dipole approximation are presented in Chapter 13 within the general approach of the Mie–Lorenz theory. Localized surface plasmon and surface phonon resonances in small nanoparticles are discussed and applications to plasmonics technology are highlighted. We also discuss light scattering from magnetic spheres and the application of the Mie–Lorenz theory to the design of three-dimensional metamaterials. Generalizations of the Mie–Lorenz scattering theory to two-dimensional and three-dimensional arrays are also addressed and examples provided in the context of aperiodic photonic bandgap structures and plasmonic molecules. The chapter ends with a brief account of the more general T-matrix null-field method for nonspherical particles.

The textbook concludes with Chapter 14, where we address the light transport and localization properties of continuous and discrete random media. The so-called microscopic or "first-principle" multiple scattering theory of random media is explained and the Dyson and Bethe–Salpeter transport equations derived under the assumption

of Gaussian disorder. The effective medium solution is obtained and its applications to the design of metamaterials are addressed. This final chapter also deals with the detailed solutions for the intensity transport in a slab geometry and introduces key ideas behind mesoscopic scattering phenomena in strongly scattering random media. The final part of the chapter discusses the applications of random scattering media to laser devices, i.e., random lasers, with uncorrelated and correlated disorder within the framework of fractional diffusion.

https://doi.org/10.1017/9781139775328.002 Published online by Cambridge University Press